ACS APPLIED MATERIALS & INTERFACES

Research Article

www.acsami.org

Surface-Engineered Graphene Navigate Divergent Biological Outcomes toward Macrophages

Nana Luo,[†,‡] Dezhi Ni,[†,‡] Hua Yue,[†] Wei Wei,*[,†] and Guanghui Ma*[,†,§]

[†]National Key Laboratory of Biochemical Engineering, Institute of Process Engineering, Chinese Academy of Sciences, Beijing, 100190, PR China

[‡]University of Chinese Academy of Sciences, Beijing 100049, PR China

[§]Collaborative Innovation Center of Chemical Science and Engineering, Tianjin 300072, PR China

Supporting Information

ABSTRACT: The "nano-bio" interface profoundly shapes the interaction between cells and nanomaterials and can even decide a cell's fate. As a nascent two-dimensional material, graphene has many unique attributes and is proposed to be a promising candidate for biomedical applications. Thus, for graphene-based applications, it is necessary to clarify how the graphene surface navigates biological outcomes when encountering "janitorial" cells (macrophages). For this purpose, we synthesized nanographene oxide (nGO) and engineered the surface with polyethylene glycol (PEG), bovine serum albumin (BSA), and poly(ether imide) (PEI). In contrast to pristine nGO, decoration with PEG and BSA hindered endocytosis and improved their benignancy toward macrophages. Contrarily, nGO-PEI commenced with favorable endocytosis but then suffered stagnation due to compromised macrophage viability. To unravel the underlying mechanisms regulating these diverse macrophage fates, we built a stepwise analysis. Compared to the others, nGO-PEI tended to interact electrostatically with mitochondria after their cellular internalization. Such an unexpected encounter disrupted the normal potential and integrity of mitochondria and then elicited an alteration in reactive oxygen species and cytochrome c. These responses further initiated the activation of the caspase family and ultimately dictated cells to undergo apoptosis. The advances described above will complement our knowledge of graphene functionality and serve to guide its application in biotechnological applications.

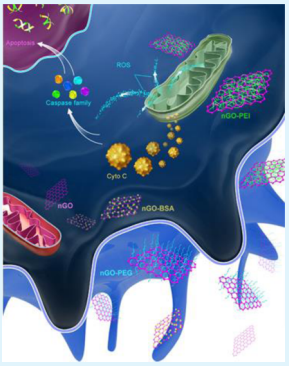

KEYWORDS: *graphene oxide, macrophage, surface engineering, biological outcomes, apoptosis*

INTRODUCTION

Nanomaterials are increasingly being actively utilized in biological applications with recent advancements in nanotechnology. Communication occurs at the instant nanomaterials and cells come into contact.[1] Such crosstalk at the "nano-bio" interface is a sophisticated process that has a profound influence on the performance of the nanomaterial and on dictating the fate of the communicating cell.[2] As for "nano-bio" interfacial properties with respect to shaping their interactions and biological outcomes, the deciding factors mainly originate from surface attributes of the nanomaterials.[3−5] Better understanding in this regard may help to tailor designated nanomaterials and enhance their performance in biological applications.

As a rising star in the field of nanomaterial science, graphene has seized tremendous attention since it first emerged.[6,7] In addition to its high thermal conductivity[8] and mechanical strength,[9,10] its unique two-dimensional plane structure also endows it with favorable attributes for biomedical applications, such as a large specific surface area for augmented drug adsorption,[11,12] stacked monolayer structure for biomolecule incorporation,[13] and intrinsic photoluminescence for live cell imaging and in vivo tracing.[14,15] When entering the body, graphene initially suffers attack by macrophages, which act as the front-line defense against foreign objects.[16,17] In this case, macrophages are the primary responders that initiate subsequent in vivo reactions[18] and profoundly determine the performance of graphene-based complexes. Thus, comprehending how surface attributes direct communication between graphene and macrophages will greatly refine graphene-based biomedical applications.

Unlike traditional zero-, one-, and three-dimensional nanomaterials, nascent two-dimensional (2D)-graphene offers a unique disposition in that its large specific surface area can facilitate the transfer of a significant amount of information at the nanobio interface. However, the biological effects of such a new dimensional nanomaterial remain unclear. Thus, a thorough dissection of this field is urgently needed. For this purpose, a comprehensive biological profile should be generated to systematically reveal how the surface properties of graphene-based nanomaterials, which give them a "synthetic identity",[19] affect their biological outcomes with respect to macrophages. Currently, the pristine graphene derivative graphene oxide (GO) was synthesized to enhance dispersion

Received: December 1, 2014
Accepted: February 18, 2015
Published: February 18, 2015

DOI: 10.1021/am5084607
ACS Appl. Mater. Interfaces 2015, 7, 5239−5247

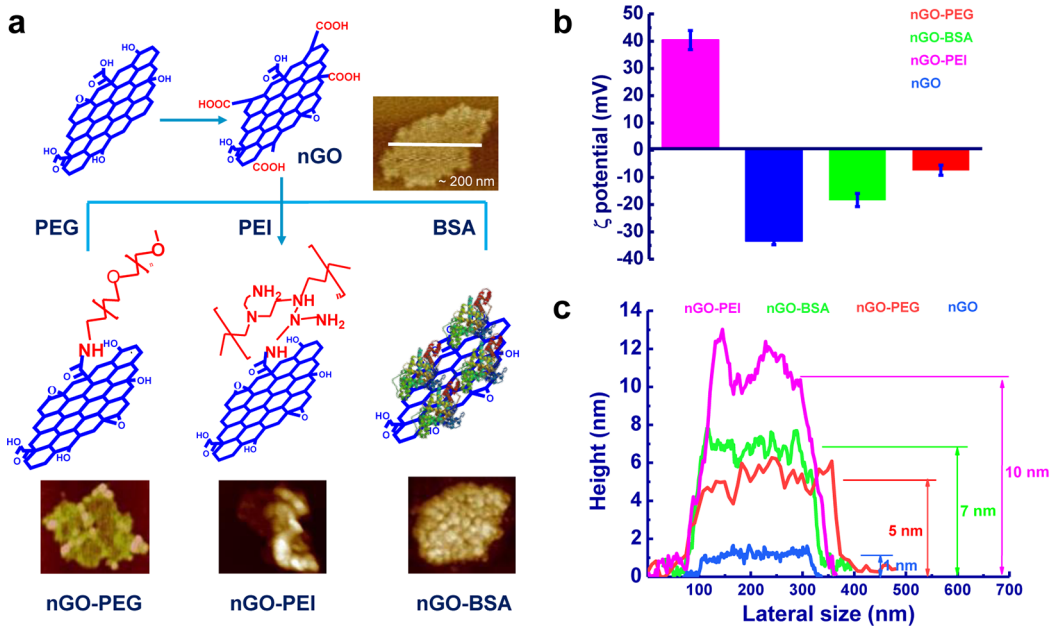

Figure 1. Schematic diagram of nGO complexes and their physical properties. (a) Schematic for engineering different nGO complexes; the insets are corresponding atomic force microscopy images. (b) Zeta potential of the different nGO complexes. (c) Surface height changes of nGO complexes before and after decoration. Data are the means ± SD with $n = 3$.

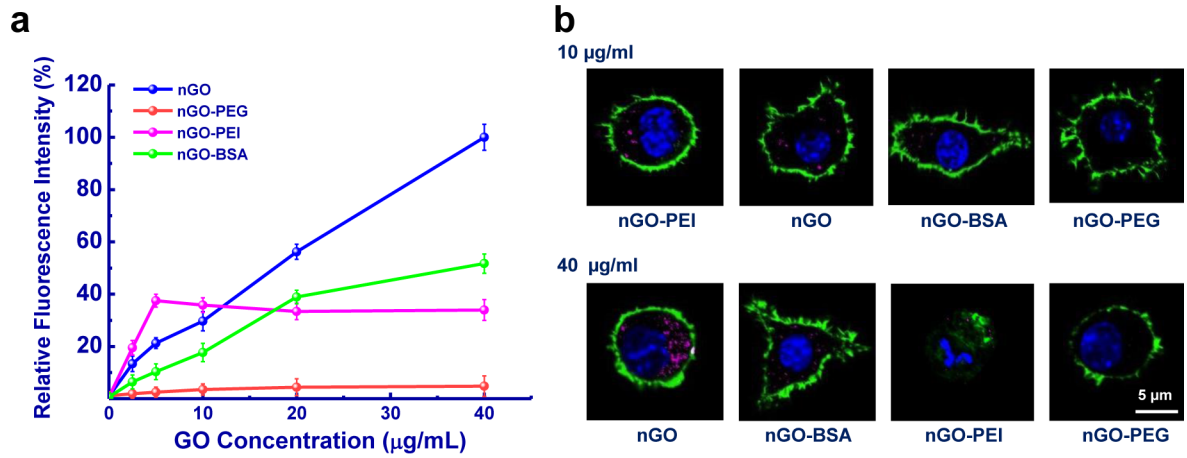

Figure 2. (a) Internalization of nGO complexes by pMØs at different doses after 24 h of coincubation. (b) Corresponding CLSM images at 10 and 40 μg/mL, where purple dots indicate nGO complexes. The images are arranged in the order of decreasing endocytosis from left to right. Data are the means ± SD with $n = 3$.

as well as facile functionalization. To study the performance of classical decorating strategies for traditional nanomaterials,[20−22] we engineered the surface of GO with polyethylene glycol (PEG), bovine serum albumin (BSA), and poly(ether imide) (PEI) (Figure 1a). Through the building of a stepwise analysis, it was found that macrophages exhibit distinct endocytotic and kinetic properties toward the different surface-engineered GO complexes. Compared to the other complexes, the preferred endocytosis of nanosized GO (nGO)-PEI was demonstrated to disturb mitochondria and eventually lead to apoptosis of macrophages by activating particular intercellular signaling cascades. Explorations in this field may contribute to the rational design of graphene-based complexes that can guarantee safety and high performance.

RESULTS AND DISCUSSION

Preparation and Characterization of nGO Complexes.

The poor solubility and high aggregation[23] of pristine graphene greatly obstructs its usefulness in biological applications. In this scenario, GO is favored for its enhanced dispersibility.[24] Herein, we produced an aqueous dispersion of ~200 nm of GO by ultrasonication and gradient centrifugation. These GO sheets were further treated with chloroacetic acid[25] and the carboxylic group was mounted from 0.9 to 28.2 mmol/g, affording abundant reaction sites for subsequent surface engineering (Figure S1 in the Supporting Information (SI)).

As shown in Figure 1b, the presence of plentiful oxygenic functional groups endowed the nGO with a much lower potential (−33.3 mV). On this basis, the chemical conjugation of PEG (Figure S2 in the SI) screened the former negative charge and closely approximated electrical neutrality (−7.36 mV). Masking BSA via hydrophobic interactions also gave

DOI: 10.1021/am5084607
ACS Appl. Mater. Interfaces 2015, 7, 5239−5247

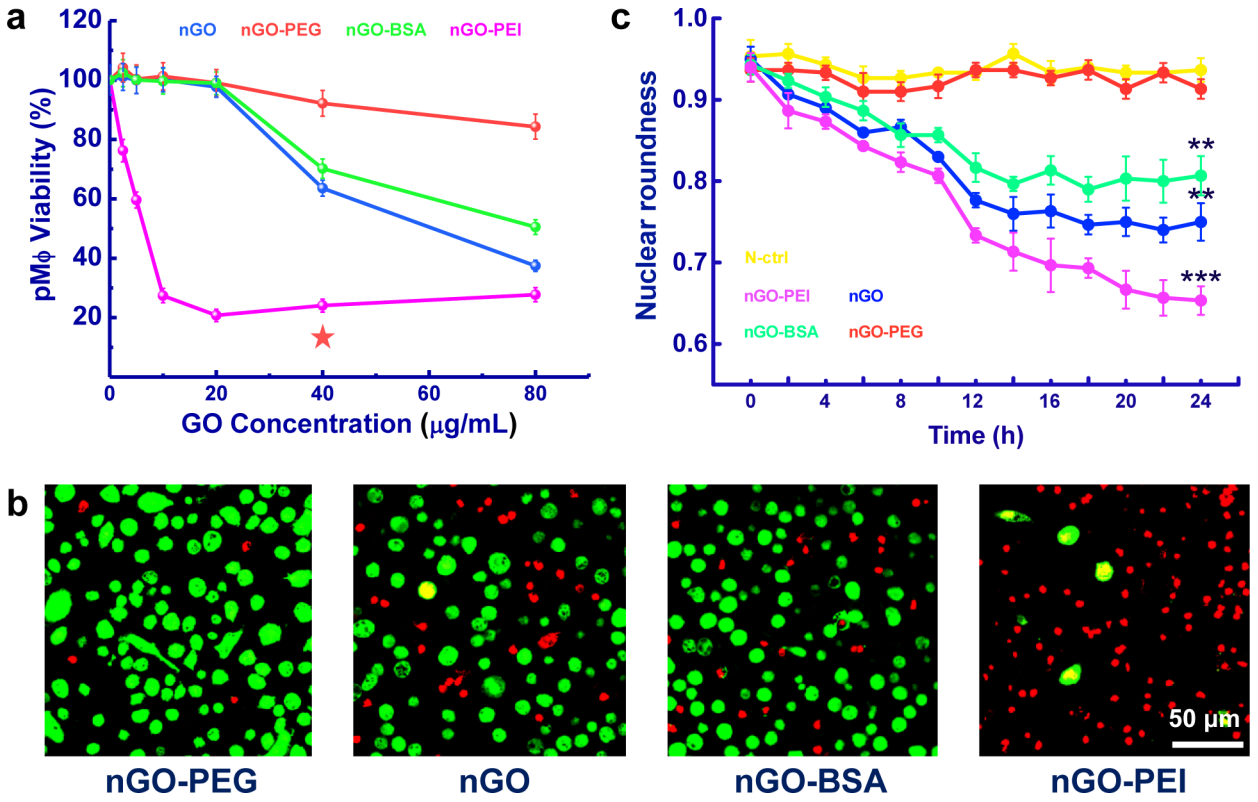

Figure 3. Impact of nGO complexes on pMØ viability after 24 h exposure. (a) Cell viability was detected by CCK-8 at a concentration gradient of 2.5, 5, 10, 20, 40, and 80 μg/mL. A significant difference in viability at 40 μg/mL is indicated by a star. (b) CLSM images stained by a LIVE/DEAD assay, where green indicates healthy macrophages and red indicates dead ones. (c) Real-time detection of nuclear roundness. Data are means ± SD with $n = 3$. *$p < 0.05$, **$p < 0.01$, and ***$p < 0.001$.

nGO-BSA a compromised negative charge (−18.3 mV), whereas absorbing PEI by electrostatic interactions completely reversed the potential to a highly positive value (+40.4 mV). Further, atomic force microscopy (AFM) imaging (Figure 1a and c) revealed the different heights and morphologies of these nGO complexes. In contrast to pristine nGO (a flat surface with ∼1 nm height), homogeneous PEG decoration lifted the height to ∼5 nm. For nGO-BSA, the mask intensified their average thickness to ∼7 nm, accompanied by an ovoid surface. Once PEI was scatteredly absorbed, the height of the nGO complex jumped to ∼10 nm. All of this data denoted the successful construction of different surface-engineered nGO complexes.

Internalization of nGO Complexes. As "big eaters", macrophages undergo prodigious endocytosis when encountered with foreign objects.[26] Thus, we evaluated endocytosis upon introducing nGO complexes at different concentrations (Figure 2a). Peritoneal macrophages (pMØs) were used throughout the study unless otherwise stated. Compared to pristine nGO, PEG camouflage greatly reduced endocytic uptake owing to the reduced number of interactions with serum components. Similarly, the hydrophilic surface layer of BSA also hindered macrophage recognition and resulted in mitigated endocytosis. This "stealth" effect supports the possible application of nGO-PEG and nGO-BSA as long-circulating drug carriers for protein, peptide, or antibody drugs, which would then rapidly be cleared after direct intravenous injection. Particularly as it relates to antitumor drug delivery, these two nGO complexes could open a time window for the passive accumulation and increased intratumoral concentration of anticancer drug cargo through leaky blood vessels. Decoration of PEI with a positive charge, on the other hand, enabled greater affinity to the cell membrane and encouraged macrophage endocytosis under 10 μg/mL. When the dose was increased further, the amount of nGO-PEI endocytosis curiously stopped climbing and even was reduced slightly. Similar results were obtained in J774A.1 cells (Figure S3a in the SI). To corroborate this data, we captured the corresponding endocytosis images with confocal laser scanning microscopy (CLSM) and Raman mapping (Figure 2b and Figure S4 in the SI). The nGO-PEI group had the highest internalization at 10 μg/mL, whereas the internalization fell below that of pristine nGO and nGO-BSA at 40 μg/mL. The confocal images also revealed disparities in cellular morphology. The nGO-PEI group caused obvious nucleus shrinkage at high concentrations, hinting at a possible connection between dosage and cytotoxicity. Further insight into the cellular internalization of nGO complexes was obtained by treating macrophages with inhibitors of clathrin-mediated endocytosis (ClME), caveolae-mediated endocytosis (CaME), macropinocytosis, and phagocytosis. These results (presented in Figure S5 in the SI) strongly suggest that ClME and phagocytosis play vital roles in the internalization of nGO complexes and that both were energy-dependent processes.

Impact of nGO Complexes on Cell Viability. The observed internalization phenomenon suggested the necessity of monitoring macrophage viability after exposure to differing concentrations of GO complexes. As shown in Figure 3a and Figure S3b in the SI, the plot of the nGO-PEI group had a distinct trend in which the cellular viability dove sharply to 20% at 10 μg/mL, whereas nGO-PEG was very benign across all of

DOI: 10.1021/am5084607
ACS Appl. Mater. Interfaces 2015, 7, 5239−5247

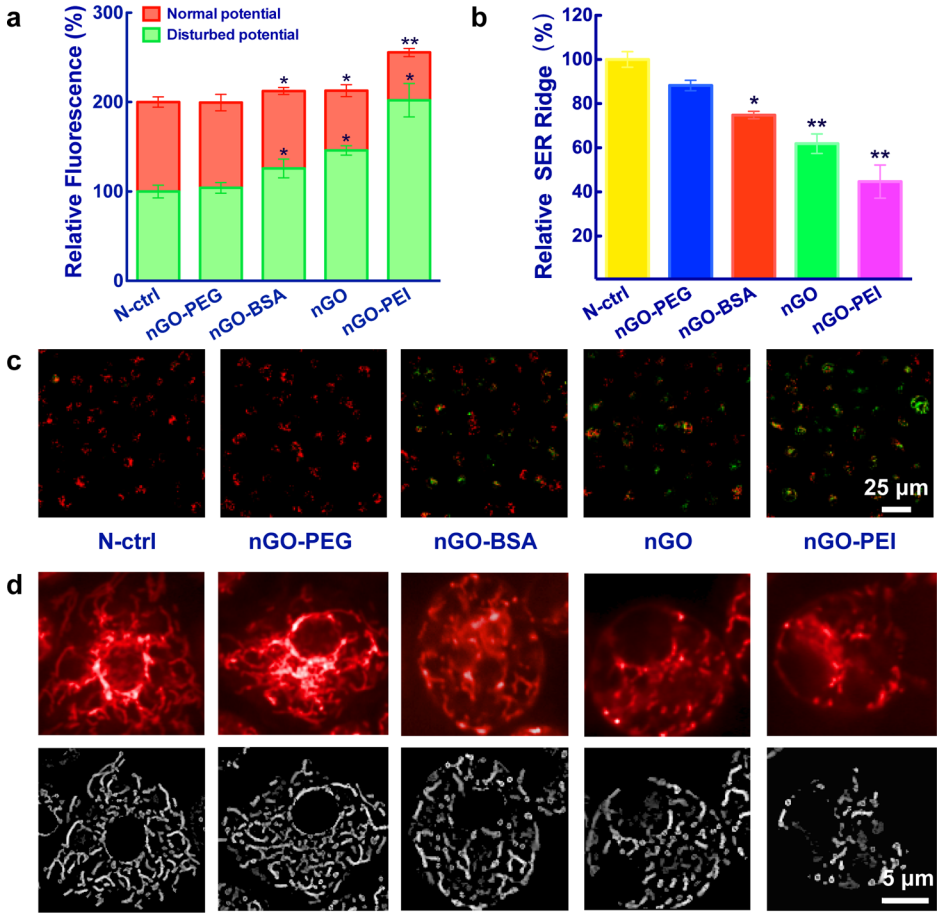

Figure 4. Influence of nGO complexes on mitochondria. (a, c) Detection of mitochondrial membrane potential (MMP) after exposing the macrophages to different nGO complexes. JC-1, an indicator of MMP, yields a red signal in healthy mitochondria but changes to green when the MMP is decreased. (b) Relative value of tubular structure after dosage calculated by the Columbus analysis system. (d) Images of mitochondria (red) and computer-simulated mitochondrial dynamic network (gray). Data are means ± SD with $n = 3$. *$p < 0.05$ and **$p < 0.01$.

the concentrations tested on the basis of its negligible endocytosis. Pristine nGO and nGO-BSA posed only moderate threats when their concentrations reached 40 μg/mL. From CLSM images of a cell viability assay at a concentration of 40 μg/mL (Figure 3b), we can directly perceive clear variation in the ratio of green to red fluorescent cells. In the nGO-PEG group, the green fluorescence, representing live cells, had absolute predominance in all signals, whereas the red fluorescence from dead cells was much denser in the other groups and was even dominant in the nGO-PEI group. As PEI-based complexes are widely used in gene transfection, these results demonstrate the potential hazard of overdosing nGO-PEI. An appropriate dosage can guarantee not only cell viability but also maximize the transfection efficacy.[27,28]

The loss of cell viability can induce consecutive morphological changes in nuclei (e.g., roundness, symmetry, and area) due to chromatin condensation and fragmentation.[29,30] In this case, monitoring nuclear morphological factors can help us to assess macrophage viability in real time and gain a deeper understanding in a temporal view. To this end, we next utilized high content screening (HCS) and monitored nuclear roundness of macrophages after exposure to different nGO complexes. In Figure 3c, the introduction of nGO-PEG maintained the nuclei at a normal state (roundness value ≈ 1.0), again confirming its good biocompatibility. But for the other three, their disturbance of macrophages caused deformations in nuclei, leading to a drop in nuclear roundness. In the nGO-PEI group, nuclear roundness had sustained falloff for 24 h, whereas it remained fairly stable in pristine nGO and the nGO-BSA group after 12 h. It is worth noting that the results in pristine nGO and nGO-BSA coincided with the trend of the time-dependent internalization curves (Figure S6 in the SI). Namely, the restricted endocytosis after 12 h stopped being detrimental to macrophage viability. Contrarily, violent uptake of nGO-PEI yielded saturation in a short amount of time (Figure S6 in the SI) and caused a continuous impact on nuclear morphology (Figure 3c), which again suggets judicious use of PEI-based complexes. Once an overdosed occurs, abundant and speedy endocytosis would result in high and persistent toxic potency.

Effects of nGO Complexes on Mitochondria. The correlation between endocytosis and cytotoxicity made us wonder what intracellular reactions caused such high discrepancies in cell viability. Thus, exploring intracellular trafficking and responses appeared to be critical to explaining the distinguished cell behaviors after exposure to different types of nGO complexes. After incubation for 24 h, large numbers of nGO-PEI were greedily devoured by macrophages, leading to the formation of many intracellular vesicles (Figure S8 in the SI). Intriguingly, nGO-PEIs attempted to pierce the vesicles and escape to cytoplasm, where there was a tremendous number of mitochondria. Given that mitochondria and nGO-

DOI: 10.1021/am5084607
ACS Appl. Mater. Interfaces 2015, 7, 5239−5247

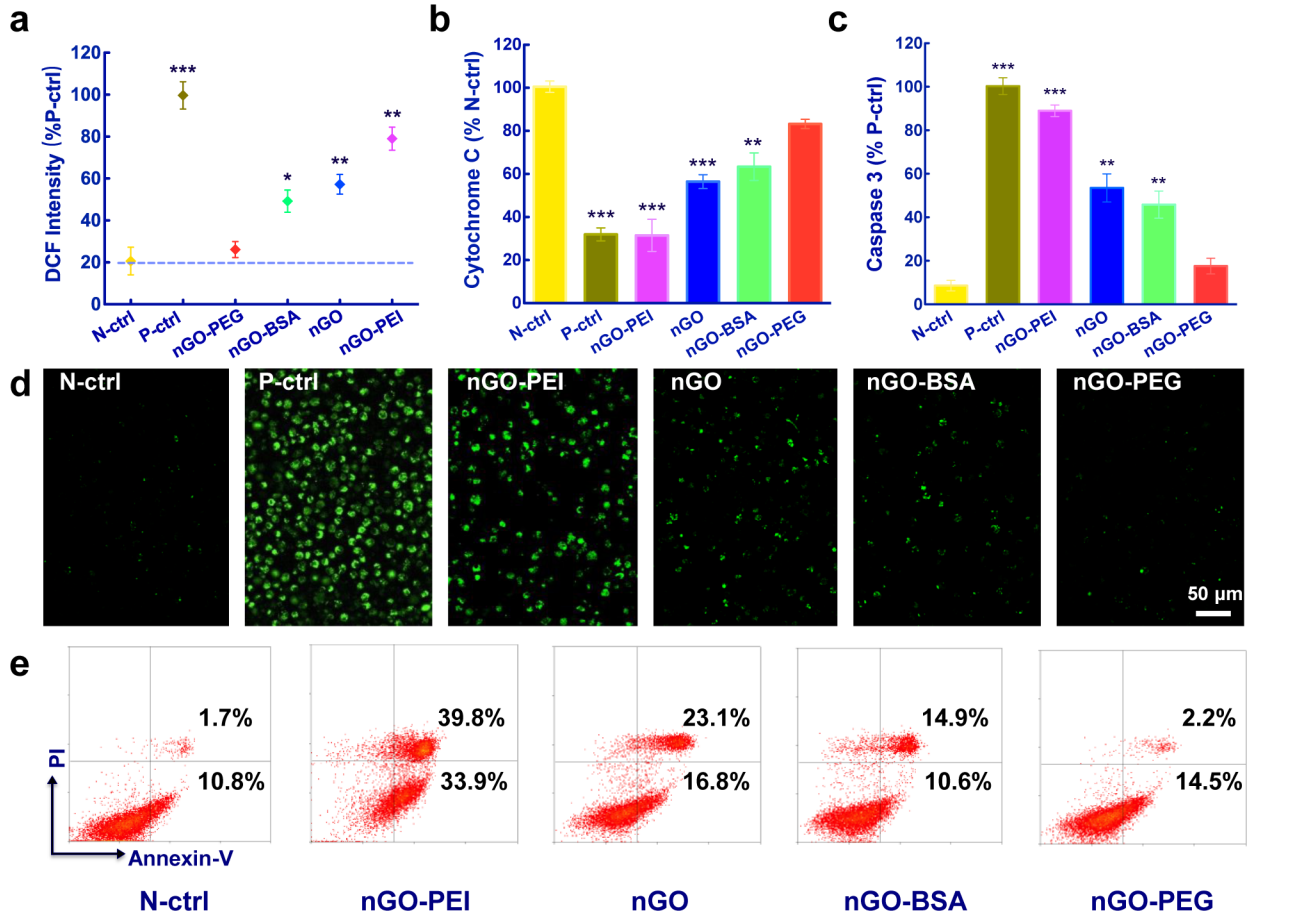

Figure 5. Downstream signaling cascade responding to nGO complexes. (a) Detection of oxidative stress by a DCF assay. (b) Reserved cytochrome c concentration in mitochondria. (c) Caspase 3 activation after different treatments and (d) corresponding CLSM images. Green spots are activated caspase 3 in macrophages. (e) Confirmation of cell apoptosis by Annexin-V/PI. The number in the right half of the plots denotes the proportion of apoptotic cells. Data are means ± SD with $n = 3$. *$p < 0.05$, **$p < 0.01$, and ***$p < 0.001$.

PEI carry the opposing charges, is is likely that the normal mitochondrial membrane potential (MMP) would be subject to electrostatic interference by nGO-PEI. The corresponding FACS histogram (Figure 4a) manifested a decreased red signal (J-aggregate from normal mitochondria) and an elevated green one (monomer fluorescence from disturbed mitochondria) in nGO-BSA, pristine nGO, and nGO-PEI groups, which is in contrast to the control and nGO-PEG groups. In accordance with the FACS data, CLSM images (Figure 4c) showed that the red signal from normal cells in the nGO-PEG group covered the whole image whereas dense green fluorescence in nGO-PEI likewise denoted collapsed potential through severe disturbance of the mitochondrial membrane.

In general, the energy in mitochondria in the form of membrane potential is distributed throughout a dynamic interconnecting network, where its highly variable morphology is maintained by constant switching between fusion (branched reticulum) and fission (fragmented structure).[31] Thus, the disturbance in MMP might imply a loss in mitochondrial integrity. With this in mind, we imaged mitochondria under HCS and reconstructed their tubular structure with the help of SER Ridge analysis in the Columbus system (Figure 4d). In healthy macrophages like those in nGO-PEG group, mitochondria are found as an elaborate branched network radiating from the nucleus. However, the addition of pristine nGO and nGO-BSA disrupted the normal fusion process and decreased their connectivity, which was further emphasized by faint staining (light gray) (Figure 4d). Even more significantly, challenging with nGO-PEI entirely broke the tubular structure, and only a few vesicular punctiform mitochondria could be observed. Furthermore, the discrepancy in mitochondrial interconnectivity was described by calculating the relative SER Ridge number percentage (Figure 4b). Their relative value indeed displayed a stepwise falloff from nGO-PEG to nGO-PEI in line with the HCS observations.

Downstream Signaling Cascade Responding to nGO Complexes. Mitochondrial impairment may give rise to disorders in related downstream signaling pathways such as reactive oxygen species (ROS), which are mainly produced by mitochondria and are essential following stimulation according to a large amount of evidence.[32] Analogous to the negative control (Figure 5a), cells were compatible with exogenous nGO-PEG, and a few scattered ROS dots stained by dichlorofluorescein (DCF) could be perceived in the image (Figure S9 in the SI). The other nGO complexes generated ROS to varying extents. In particular, nGO-PEI remarkably actuated the production of ROS by reaching up to 75% of the positive control, which greatly exceeded the steady state. Thus far, it is logical to presume that mitochondrial depolarization along with a decrease in MMP may disrupt antioxidant defenses and accelerate ROS levels.

DOI: 10.1021/am5084607
ACS Appl. Mater. Interfaces 2015, 7, 5239−5247

Cytochrome c (Cyt c) is usually located inside healthy mitochondria to perform its function, whereas mitochondrial dysfunction induced by oxidative stress compels its release.[33] Thus, disrupted mitochondria suggested that we should monitor the intracellular location of Cyt c (Figure 5b). As opposed to that in the negative and nGO-PEG groups, the addition of nGO-PEI caused abundant translocation of Cyt c (close to positive) from mitochondria to the cytosol. Correspondingly, we could perceive barely visible fluorescence of reserved Cyt c in the nGO-PEI group, yet widely distributed red staining in the nGO-PEG group (Figure S10 in the SI). Pristine nGO and nGO-BSA also elicited ∼40% Cyt c transference and had a moderate level of fluorescence remaining in the mitochondria (Figure S10 in the SI). Similar results of released Cyt c were obtained by Western blotting analysis (Figure S11 in the SI).

Serving as a convergence point for the aforementioned downstream signaling pathways, caspase 3 is crucial to decide the fate of a cell.[34] To further determine whether it is involved in the regulation by the nGO complexes, we next evaluated its activation levels. In Figure 5c, caspase 3 was shown to be activated by ∼80% after introducing nGO-PEI, which was adjacent to the positive control. Activated caspase 3 was gradually decreased in the order of pristine nGO, nGO-BSA, and nGO-PEG, which positively correlates with the tendencies described above. The results were also confirmed by confocal imaging. The green fluorescent signal emitting from a carboxyfluorescein group (FAM) reported activated caspase 3, which faded out from left to right (Figure 5d). Western blotting (Figure S11 in the SI) provided concordant results based on the protein levels of procaspase 3. To determine whether the activation of caspase 3 was required for nGO-PEI-induced cell death, we pretreated macrophages with a caspase inhibitor (Figure S12 in the SI). It is found that cell death was partially reversed by dropping the active caspase 3 level over 50%, arguing its importance in the nGO-PEI-mediated signaling pathway.

Caspase 3 activation has been demonstrated to be heavily involved in programmed cell death.[35] This prompted us to assess the role of apoptosis in nGO complex-induced cell viability. Usually, apoptotic cell death is accompanied by a change in the plasma membrane structure by surface exposure of phosphatidylserine (PS),[36] which can be identified by Annexin-V. Furthermore, the addition of PI can help to further differentiate early from late apoptotic cells. In Figure 5e, after exposure to nGO-PEI, the number of early apoptotic macrophages (Annexin V positive) tripled compared to that of the negative control and nearly one-third of the cells went into late apoptosis (double positive). In parallel, pristine nGO and nGO-BSA also engendered some apoptotic macrophages. On the basis of its outstanding benignity, the nGO-PEG group exhibited a nearly double negative result, illustrating the health of the treated macrophages. Taken together, apoptosis played a major role in the decreased macrophage viability induced by nGO, which in turn validated the accuracy of the signaling pathway we proposed above.

CONCLUSIONS AND PERSPECTIVES

After stepwise explorations, we determined the mechanism by which nGO complexes navigate macrophage biological outcomes and proposed a schematic of the intracellular pathway (Figure 6). Surface engineering of nGO sheets altered their synthetic identity and varied their levels of endocytosis over a wide range. Positively charged nGO-PEI was more likely to bind on the surface of the macrophage membrane to facilitate endocytosis. BSA adsorption, on the other hand, eliminated the binding of serum components to the GO surface thereby lowering the level of endocytosis. This "stealth" effect was further improved in nGO-PEG complexes, which almost completely inactivated endocytosis, removing the opportunity for a subsequent intracellular response. Focusing on the intracellular context, nGO-PEI was more likely to interact with mitochondria than nGO-BSA or pristine nGO, disrupting the mitochondria by eliciting a sharp decrease in membrane potential and structural connectivity. Such impairments on mitochondria were followed by a fluctuation in intracellular ROS and release of Cyt c from the mitochondria. Cyt c translocation subsequently initiated activation of the caspase family and ultimately dictated macrophages to undergo apoptosis.

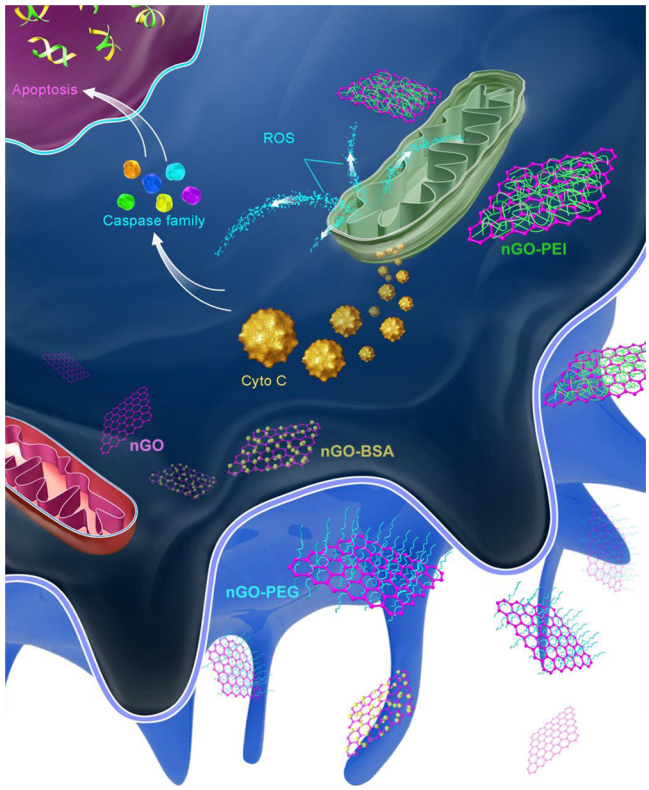

Figure 6. Schematic illustration of the distinct intracellular pathways in a macrophage after exposure to different nGO complexes. Decoration by PEG almost completely ceased endocytosis and caused nGO-PEGs to wander extracellularly. After being phagocytized, nGO-PEI was more apt to interact with mitochondria and activate the downstream signaling cascade.

As more and more engineered GO nanomaterials become favored because of their multiple functionality,[37,38] the results described above caution the use of tunable attributes to prevent the introduction of confusing biological complications in attempting to accomplish specific missions. In this respect, fully unveiling the dispositions at the nanobio interface is indispensible and significant. Induced intracellular responses in macrophages will be further refined in our future work by broadening the approach to include cellular stress, cytokine production, and potential inflammation.[39,40] Beyond this, given that macrophages actively participate in immune response, a new avenue may be opened for developing safe and efficient

DOI: 10.1021/am5084607
ACS Appl. Mater. Interfaces 2015, 7, 5239−5247

vaccines. Advances in these fields will definitely augment the development of GO-based nanomaterials for various biomedical applications.

EXPERIMENTAL SECTION

Reagents and Materials. Methoxypolyethylene glycol amine (mPEG-NH_2, M_w = 2000) was obtained from Beijing Jenkem Technology. Poly(ether imide) (PEI) and bovine serum albumin (BSA) were purchased from Sigma and Roche Co., respectively. Gibco Dulbecco's phosphate-buffered saline (D-PBS), Dulbecco's modified Eagle's medium (DMEM), rhodamine-phalloidin, Hoechst 33342, MitoTracker Red, LIVE/DEAD Cell Viability Kit, Annexin V/Dead Cell Apoptosis Kit, Vybrant FAM Caspase-3 and -7 Assay Kit, and MitoProbeTM JC-1 Assay Kit were all acquired from Invitrogen. Flow Cytometric Cytochrome c Calbiochem Release Kit, PVDF membranes, chlorpromazine, genistein, amiloride, and cytochalasin D were bought from EMD Millipore. Cell Counting Kit-8 (CCK8), Reactive Oxygen Species (ROS) Assay Kit, staurosporine, Z-VAD-FMK, SDS-PAGE gels, and BeyoECL Plus were ordered from Beyotime Institute. 1-Ethyl-3-(3-dimethylamino-propyl) carbodiimide (EDC) was purchased from J&K Chemical Ltd. β-actin was purchased from Santa Cruz Biotechnology. Anti-cytochrome c and procaspase 3 antibodies were purchased from Abcam. GO powders were kind gifts from Ding Ma's Group at Peking University. All other reagents were of analytic grade.

Animals and Cells. C57BL/6 mice were ordered from Charles River Laboratories (USA). All animal experiments were performed in compliance with the institutional ethics committee regulations and guidelines on animal welfare. Peritoneal macrophages were harvested from stimulated C57BL/6 mice according to a standard protocol,[41] and the murine macrophage cell line J774A.1 was supplied by ATCC (American Type Culture Collection). Cells were cultured with DMEM cell culture medium with added penicillin (100 U/mL), streptomycin (100 U/mL), and 10% fetal bovine serum (FBS) in a humidified incubator at 37 °C and 5% CO_2.

Synthesis and Characterization of the nGO Complexes. *Pristine nGO.* GO powder was added to deionized water and sufficiently sonicated for 7 h to prepare a highly dispersive GO solution. Then, GO sheets were sorted by size through gradient centrifugation and uniform GO sheets of the desired size (~200−300 nm) were obtained at 50000−70000*g* centrifugal force. To increase the number of carboxylic acid moieties for further functionalization, GO sheets (50 mL, 100 μg/mL) were added to a solution containing 1 M chloroacetic acid and 3 M NaOH. After reacting for 70 min at room temperature with stirring, the reaction was stopped by adjusting the pH to neutral with 6 N HCl.[25] Finally, the nanosized GO was purified by repeated suspensions and centrifugations with deionized (DI) water.

The carboxyl group densities before and after oxidization were calculated from a conductance curve obtained by conductive titration according to the following equation: carboxyl groups intensity (mmol/g) = $M(V_2 - V_1)/W$, where M (mol/L) is the concentration of sodium hydroxide (NaOH), $(V_2 - V_1)$ (mL) is the linear fitting volume of NaOH, and W (g) is the GO quality.

nGO-PEG. PEGylation procedures of pristine nGO were mainly consulted from a previous report.[42] First, EDC (20 mM) was added to the pristine nGO suspension (~500 μg/mL) and sonicated for 15 min. Immediately, mPEG-NH_2 (10 mg/mL) was added and allowed to react overnight. The final product (nGO-PEG) was harvested by centrifugation at 70000*g* after repeated washing by DI water. The successful coupling of mPEG-NH_2 to pristine nGO was verified by analysis using a FT/IR-660 Fourier transform infrared spectrometer (Jasco Co.).

nGO-PEI. Preparation of nGO-PEI was carried out according to a previously reported method.[43] In detail, a solution of branched PEI (M_w = 25000, 1 mg/mL) was slowly added to a pristine nGO solution (1 mg/mL) with stirring to achieve a final nGO/PEI weight ratio of 1:4. The mixture solution was immediately sonicated for 10 min and stirred overnight. Then, the nGO-PEI complex was obtained after repeated washing with DI water.

nGO-BSA. A mixture solution of pristine nGO (0.1 mg/mL) and BSA (20 mg/mL) was prepared and rotated at room temperature for 24 h.[23] Excess BSA was removed by multiple centrifugations at 70000*g*, and the product was resuspended in DI water.

Characterization of nGO-complexes for lateral sizes, morphologies, and heights was performed on a Dimension FastScan AFM microscope (Bruker). The zeta potential of the nGO complexes was determined by Zeta Sizer (Nano Series, Malvern).

Cellular Uptake Studies. pMØ and J774A.1 cells were cultured in 24-well plates, and different nGO complexes of appointed concentrations were added to the cell culture medium at particular intervals. After incubation, the cells were collected and washed with PBS buffer three times. Taking advantage of graphene's intrinsic photoluminescence, the intracellular nGO complex amounts were detected using CyAn ADP 9 color flow cytometry (FACS, Beckman Coulter) via the PE-Cy7 channel. As BSA decreased the fluorescent intensity to ~20% that of pristine nGO, the final intensity of nGO-BSA was made with a corresponding compensation. PEI and PEG had little impact on the fluorescent intensity.

To visualize nGO internalization, pMØs were seeded (1×10^5/mL) in a Petri dish and incubated with nGO complexes at 10 and 40 μg/mL for 24 h. Then, the cells were washed with PBS three times, fixed in 3.7% paraformaldehyde for 30 min, and 0.1% Triton X-100 for 5 min. The cytoskeleton and nuclei were subsequently separately stained with rhodamine-phalloidin (green pseudocolor in images) and Hoechst, respectively, for 20 min at room temperature. Images were captured by an Ultraview VoX cell imaging system (PerkinElmer). For Raman mapping, the processing methods for cell fixation were the same as described above. After the cells were rinsed with PBS three times, Raman images were taken on a laser Raman microscope (Raman-11, Nanophoton) at 532 nm excitation.

For the internalization pathways of the nGO complexes to be evaluated, macrophages were preincubated with specific inhibitors as previously reported.[40] Briefly, they were pretreated separately with chlorpromazine (10 μg/mL), genistein (200 μM), amiloride (50 μg/mL), and cytochalasin D (10 μM) for 1 h. The media was then changed to fresh media containing nGO complexes for a 24 h incubation, and the cells were then analyzed by flow cytometry.

To further study the intracellular trafficking of nGO-PEI, we challenged pMØ cells with 40 μg/mL nGO-PEI for 24 h, and the corresponding images were taken by a JEM-1400 transmission electron microscope (TEM, JEOL).

Biocompatibility of nGO Complexes. Typically, pMØ and J774A.1 cells were cultured in 96-well plate. Subsequently, serial dilutions of different nGO solutions ranging from 0 to 80 μg/mL were added. After a 24 h incubation, the viability of the cells was analyzed by a CCK-8 assay and a LIVE/DEAD cell viability kit according to the instructions provided by the manufacturers.

Observation of Morphological Variety in the Nucleus and Mitochondria. pMØs were seeded in a 96-well PerkinElmer cell carrier and stained with Hoechst (3 μg/mL) for 2 h. Then, the culture medium was replaced by DMEM mixed with the different nGO complexes at 40 μg/mL. For the variety in nucleur morphology to be monitored in real time, images were taken every 2 h over a duration of 24 h by HCS (Opera, PerkinElmer).

To detect morphological changes in mitochondria, we pretreated pMØ cells with nGO complexes at 40 μg/mL for 23 h, and MitoTracker Red (200 nM) was added to stain for 1 h. Then, mitochondrial morphologies were analyzed by the HCS system at 24 h. Nuclear roundness and the SER Ridge, indicating connectivity of the mitochondria, were analyzed in a Columbus analysis system (PerkinElmer) by building the corresponding blocks.

Downstream Signaling Cascade Study. For the detection of mitochondrial membrane potential (JC-1 assay), ROS (DCFH-DA Assay), cytochrome c, caspase 3/7, and cell apoptosis (Annexin V-FITC/PI), pMØ cells were collected after coincubation with nGO complexes at 40 μg/mL for 24 h followed by treatments according to the relevant instructions. Finally, the samples were analyzed on a flow

DOI: 10.1021/am5084607
ACS Appl. Mater. Interfaces 2015, 7, 5239−5247

cytometer with 488/561 nm excitation, and the corresponding images were taken by confocal microscopy imaging (Ultraview VoX). During the study, macrophages treated with 0.2 mM staurosporine served as positive controls for cytochrome c and caspase 3 detection. Macrophages were pretreated with the caspase inhibitor Z-VAD-FMK (20 μM) for 30 min in the apoptosis inhibition assay.

Western Blot for Cytochrome c and Procaspase 3. After a 24 h incubation with nGO complexes, macrophages were lysed with RIPA buffer containing 1× halt protease inhibitor cocktail, and cell lysates were obtained after centrifugation. For immunoblotting analysis, lysates were loaded onto 4−12% SDS-PAGE gels, and subsequently transferred onto a PVDF membrane. The membrane was blocked with 5% skim milk for 2 h and incubated overnight with primary antibodies for β-actin (1:1,000), Cyt c (1:2,000), and procaspase 3 (1:1000). The membranes were then incubated with horseradish peroxidase-conjugated antirabbit IgG (1:2,000). After visualizing the proteins by ECL, we analyzed the membranes using a DNR bio-imaging system (MF-ChemiBIS 3.2).

Statistical Analysis. Statistical evaluations of the data were performed by Student's t test for two groups and one way ANOVA for multiple groups. All results were expressed as the mean ± standard deviation (SD). $p < 0.05$ was considered statistical significant.

■ ASSOCIATED CONTENT

Ⓢ Supporting Information

Additional conductance curves for calculating carboxylic groups, FTIR spectra of nGO-PEG, internalization and viability assays of J774A.1 cells, Raman mappings, evaluation of the endocytic pathway, internalization kinetics of pMØ, FACS data of Live/Dead viability assay, TEM images of nGO-PEI, confocal images of ROS and Cyt c, Western blot of procaspase 3 and released Cyt c, and a caspase 3 inhibition assay. This material is available free of charge via the Internet at http://pubs.acs.org.

■ AUTHOR INFORMATION

Corresponding Authors

*E-mail: weiwei@home.ipe.ac.cn.
*E-mail: ghma@home.ipe.ac.cn.

Notes

The authors declare no competing financial interest.

■ ACKNOWLEDGMENTS

This work was supported by the National Basic Research Program of China (973 Program, 2013CB531505), National Nature Science Foundation of China (81302704), and Beijing Nova Program (Z141102001814066).

■ REFERENCES

(1) Nel, A. E.; Madler, L.; Velegol, D.; Xia, T.; Hoek, E. M. V.; Somasundaran, P.; Klaessig, F.; Castranova, V.; Thompson, M. Understanding Biophysicochemical Interactions at the Nano-Bio Interface. *Nat. Mater.* **2009**, *8*, 543−557.

(2) Murphy, W. L.; McDevitt, T. C.; Engler, A. J. Materials as Stem Cell Regulators. *Nat. Mater.* **2014**, *13*, 547−557.

(3) Albanese, A.; Tang, P. S.; Chan, W. C. W. The Effect of Nanoparticle Size, Shape, and Surface Chemistry on Biological Systems. *Annu. Rev. Biomed. Eng.* **2012**, *14*, 1−16.

(4) Alkilany, A. M.; Lohse, S. E.; Murphy, C. J. The Gold Standard: Gold Nanoparticle Libraries to Understand the Nano-Bio Interface. *Acc. Chem. Res.* **2013**, *46*, 650−661.

(5) Walkey, C. D.; Olsen, J. B.; Guo, H. B.; Emili, A.; Chan, W. C. W. Nanoparticle Size and Surface Chemistry Determine Serum Protein Adsorption and Macrophage Uptake. *J. Am. Chem. Soc.* **2012**, *134*, 2139−2147.

(6) Geim, A. K.; Novoselov, K. S. The Rise of Graphene. *Nat. Mater.* **2007**, *6*, 183−191.

(7) Dreyer, D. R.; Ruoff, R. S.; Bielawski, C. W. From Conception to Realization: An Historial Account of Graphene and Some Perspectives for Its Future. *Angew. Chem., Int. Ed.* **2010**, *49*, 9336−9344.

(8) Balandin, A. A.; Ghosh, S.; Bao, W. Z.; Calizo, I.; Teweldebrhan, D.; Miao, F.; Lau, C. N. Superior Thermal Conductivity of Single-Layer Graphene. *Nano Lett.* **2008**, *8*, 902−907.

(9) Lee, C.; Wei, X. D.; Kysar, J. W.; Hone, J. Measurement of the Elastic Properties and Intrinsic Strength of Monolayer Graphene. *Science* **2008**, *321*, 385−388.

(10) Chen, H.; Muller, M. B.; Gilmore, K. J.; Wallace, G. G.; Li, D. Mechanically Strong, Electrically Conductive, and Biocompatible Graphene Paper. *Adv. Mater.* **2008**, *20*, 3557−3561.

(11) Yang, K.; Feng, L. Z.; Shi, X. Z.; Liu, Z. Nano-Graphene in Biomedicine: Theranostic Applications. *Chem. Soc. Rev.* **2013**, *42*, 530−547.

(12) Goenka, S.; Sant, V.; Sant, S. Graphene-Based Nanomaterials for Drug Delivery and Tissue Engineering. *J. Controlled Release* **2014**, *173*, 75−88.

(13) Wang, Y.; Li, Z. H.; Wang, J.; Li, J. H.; Lin, Y. H. Graphene and Graphene Oxide: Biofunctionalization and Applications in Biotechnology. *Trends Biotechnol.* **2011**, *29*, 205−212.

(14) Sun, X. M.; Liu, Z.; Welsher, K.; Robinson, J. T.; Goodwin, A.; Zaric, S.; Dai, H. J. Nano-Graphene Oxide for Cellular Imaging and Drug Delivery. *Nano Res.* **2008**, *1*, 203−212.

(15) Gollavelli, G.; Ling, Y. C. Multi-Functional Graphene as an in Vitro and in Vivo Imaging Probe. *Biomaterials* **2012**, *33*, 2532−2545.

(16) Gordon, S. The Macrophage: Past, Present and Future. *Eur. J. Immunol.* **2007**, *37*, S9−S17.

(17) Anderson, J. M.; Rodriguez, A.; Chang, D. T. Foreign Body Reaction to Biomaterials. *Semin. Immunol.* **2008**, *20*, 86−100.

(18) Kagan, V. E.; Tyurina, Y. Y.; Tyurin, V. A.; Konduru, N. V.; Potapovich, A. I.; Osipov, A. N.; Kisin, E. R.; Schwegler-Berry, D.; Mercer, R.; Castranova, V.; Shvedova, A. A. Direct and Indirect Effects of Single Walled Carbon Nanotubes on RAW 264.7 Macrophages: Role of Iron. *Toxicol. Lett.* **2006**, *165*, 88−100.

(19) Walkey, C. D.; Chan, W. C. W. Understanding and Controlling the Interaction of Nanomaterials with Proteins in a Physiological Environment. *Chem. Soc. Rev.* **2012**, *41*, 2780−2799.

(20) Liu, Z.; Cai, W. B.; He, L. N.; Nakayama, N.; Chen, K.; Sun, X. M.; Chen, X. Y.; Dai, H. J. In Vivo Biodistribution and Highly Efficient Tumour Targeting of Carbon Nanotubes in Mice. *Nat. Nanotechnol.* **2007**, *2*, 47−52.

(21) Cedervall, T.; Lynch, I.; Lindman, S.; Berggard, T.; Thulin, E.; Nilsson, H.; Dawson, K. A.; Linse, S. Understanding the Nanoparticle-Protein Corona Using Methods to Quantify Exchange Rates and Affinities of Proteins for Nanoparticles. *Proc. Natl. Acad. Sci. U.S.A.* **2007**, *104*, 2050−2055.

(22) Xia, T. A.; Kovochich, M.; Liong, M.; Meng, H.; Kabehie, S.; George, S.; Zink, J. I.; Nel, A. E. Polyethyleneimine Coating Enhances the Cellular Uptake of Mesoporous Silica Nanoparticles and Allows Safe Delivery of siRNA and DNA Constructs. *ACS Nano* **2009**, *3*, 3273−3286.

(23) Liu, J. B.; Fu, S. H.; Yuan, B.; Li, Y. L.; Deng, Z. X. Toward a Universal "Adhesive Nanosheet" for the Assembly of Multiple Nanoparticles Based on a Protein-Induced Reduction/Decoration of Graphene Oxide. *J. Am. Chem. Soc.* **2010**, *132*, 7279−7281.

(24) Konkena, B.; Vasudevan, S. Understanding Aqueous Dispersibility of Graphene Oxide and Reduced Graphene Oxide through pK_a Measurements. *J. Phys. Chem. Lett.* **2012**, *3*, 867−872.

(25) Yue, Z. G.; Lv, P. P.; Yue, H.; Gao, Y. J.; Ma, D.; Wei, W.; Ma, G. H. Inducible Graphene Oxide Probe for High-Specific Tumor Diagnosis. *Chem. Commun. (Cambridge, U.K.)* **2013**, *49*, 3902−3904.

(26) Erturk-Hasdemir, D.; Silverman, N. Eater: A Big Bite into Phagocytosis. *Cell* **2005**, *123*, 190−192.

(27) Chen, B. A.; Liu, M.; Zhang, L. M.; Huang, J.; Yao, J. L.; Zhang, Z. J. Polyethylenimine-Functionalized Graphene Oxide as an Efficient Gene Delivery Vector. *J. Mater. Chem.* **2011**, *21*, 7736−7741.

DOI: 10.1021/am5084607
ACS Appl. Mater. Interfaces 2015, 7, 5239−5247

(28) Feng, L. Z.; Yang, X. Z.; Shi, X. Z.; Tan, X. F.; Peng, R.; Wang, J.; Liu, Z. Polyethylene Glycol and Polyethylenimine Dual-Functionalized Nano-Graphene Oxide for Photothermally Enhanced Gene Delivery. *Small* **2013**, *9*, 1989−1997.
(29) Filippi-Chiela, E. C.; Oliveira, M. M.; Jurkovski, B.; Callegari-Jacques, S. M.; da Silva, V. D.; Lenz, G. Nuclear Morphometric Analysis (NMA): Screening of Senescence, Apoptosis and Nuclear Irregularities. *PLoS One* **2012**, *7*, e42522-1−e42522-10.
(30) Ziegler, U.; Groscurth, P. Morphological Features of Cell Death. *News Physiol. Sci.* **2004**, *19*, 124−128.
(31) Karbowski, M.; Youle, R. J. Dynamics of Mitochondrial Morphology in Healthy Cells and During Apoptosis. *Cell Death Differ.* **2003**, *10*, 870−880.
(32) Pan, Y.; Leifert, A.; Ruau, D.; Neuss, S.; Bornemann, J.; Schmid, G.; Brandau, W.; Simon, U.; Jahnen-Dechent, W. Gold Nanoparticles of Diameter 1.4 nm Trigger Necrosis by Oxidative Stress and Mitochondrial Damage. *Small* **2009**, *5*, 2067−2076.
(33) Zhou, F. F.; Wu, S. N.; Wu, B. Y.; Chen, W. R.; Xing, D. Mitochondria-Targeting Single-Walled Carbon Nanotubes for Cancer Photothermal Therapy. *Small* **2011**, *7*, 2727−2735.
(34) Lakhani, S. A.; Masud, A.; Kuida, K.; Porter, G. A.; Booth, C. J.; Mehal, W. Z.; Inayat, I.; Flavell, R. A. Caspases 3 and 7: Key Mediators of Mitochondrial Events of Apoptosis. *Science* **2006**, *311*, 847−851.
(35) Lavrik, I. N.; Golks, A.; Krammer, P. H. Caspases: Pharmacological Manipulation of Cell Death. *J. Clin. Invest.* **2005**, *115*, 2665−2672.
(36) Zwaal, R. F. A.; Comfurius, P.; Bevers, E. M. Surface Exposure of Phosphatidylserine in Pathological Cells. *Cell. Mol. Life Sci.* **2005**, *62*, 971−988.
(37) Veiseh, O.; Gunn, J. W.; Zhang, M. Q. Design and Fabrication of Magnetic Nanoparticles for Targeted Drug Delivery and Imaging. *Adv. Drug Delivery Rev.* **2010**, *62*, 284−304.
(38) Sanvicens, N.; Marco, M. P. Multifunctional Nanoparticles-Properties and Prospects for their Use in Human Medicine. *Trends Biotechnol.* **2008**, *26*, 425−433.
(39) Dobrovolskaia, M. A.; Mcneil, S. E. Immunological Properties of Engineered Nanomaterials. *Nat. Nanotechnol.* **2007**, *2*, 469−478.
(40) Yue, H.; Wei, W.; Yue, Z. G.; Wang, B.; Luo, N. N.; Gao, Y. J.; Ma, D.; Ma, G. H.; Su, Z. G. The Role of the Lateral Dimension of Graphene Oxide in the Regulation of Cellular Responses. *Biomaterials* **2012**, *33*, 4013−4021.
(41) Major, J.; Fletcher, J. E.; Hamilton, T. A. IL-4 Pretreatment Selectively Enhances Cytokine and Chemokine Production in Lipopolysaccharide-Stimulated Mouse Peritoneal Macrophages. *J. Immunol.* **2002**, *168*, 2456−2463.
(42) Liu, Z.; Robinson, J. T.; Sun, X. M.; Dai, H. J. PEGylated Nanographene Oxide for Delivery of Water-Insoluble Cancer Drugs. *J. Am. Chem. Soc.* **2008**, *130*, 10876−10877.
(43) Feng, L. Z.; Zhang, S. A.; Liu, Z. A. Graphene Based Gene Transfection. *Nanoscale* **2011**, *3*, 1252−1257.

DOI: 10.1021/am5084607
ACS Appl. Mater. Interfaces 2015, 7, 5239−5247